Dalton Transactions

Synthesis, Crystal and Electronic Structures, Linear and Nonlinear Optical Properties, and Photocurrent Response of Oxyhalides $CeHaVIO_4$ (Ha=Cl, Br; VI=Mo, W)

Journal:	*Dalton Transactions*
Manuscript ID	DT-ART-10-2023-003640.R1
Article Type:	Paper
Date Submitted by the Author:	06-Dec-2023
Complete List of Authors:	Jiao, Zixian; Wichita State University, Chemistry and Biochemistry Quah, Jasmine; Wichita State University, Chemistry and Biochemistry Syed, Tajamul Hussain; Wichita State University Wei, Wei; Wichita State University, Mechanical Engineering Zhang, Bingbing; Hebei University, College of Chemistry and MaterialsScience; HBU Wang, Fei; Missouri State University, Chemistry and Biochemistry Wang, Jian; Wichita State University, Chemistry

Synthesis, Crystal and Electronic Structures, Linear and Nonlinear Optical Properties, and Photocurrent Response of Oxyhalides $CeHaVIO_4$ (Ha=Cl, Br; VI=Mo, W)

Zixian Jiao [a], Jasmine Quah [a], Tajamul Hussain Syed [b], Wei Wei [b], Bingbing Zhang [c], Fei Wang [d, *], Jian Wang [a, *]

[a] *Department of Chemistry and Biochemistry, Wichita State University, Wichita, Kansas 67260, United States*

[b] *Department of Mechanical Engineering, Wichita State University, Wichita, Kansas 67260, United States*

[c] *College of Chemistry and Environmental Science, Hebei University, Key Laboratory of Analytical Science and Technology of Hebei Province, Baoding 071002, China*

[d] *Department of Chemistry and Biochemistry, Missouri State University, Springfield, Missouri, 65897, United States*

Abstract

Four heteroanionic oxyhalides, $CeClMoO_4$, $CeBrMoO_4$, $CeClWO_4$, and $CeBrWO_4$, have been studied as multifunctional materials, which combine good second harmonic generation (SHG) response and photocurrent signals. Millimeter-sized $CeHaVIO_4$ (Ha=Cl, Br; VI=Mo, W) crystals were grown by halide salt flux. The crystal structure of $CeHaVIO_4$ crystals was accurately determined by single crystal X-ray diffraction. $CeClMoO_4$, $CeBrMoO_4$, and $CeBrWO_4$ are isostructural to each other, which crystallize in the acentric $LaBrMoO_4$ structure type. $CeClWO_4$ crystallizes in a new structure type with unit cell parameters of a=19.6059(2) Å, b=5.89450(10) Å, c=7.80090(10) Å, β=101.4746(8)°. The bandgaps of $CeHaVIO_4$ fall into the range of 2.8(1)-3.1(1) eV, which are much smaller than the isotypic $LaHaVIO_4$ (Ha=Cl, Br; VI=Mo, W) of 3.9(1)-4.3(1) eV. The narrowing of bandgaps in $CeHaVIO_4$ originates from the presence of partially filled *4f* orbitals of cerium atoms, which was confirmed by density functional theory (DFT) calculations. The moderate bandgaps make $CeHaVIO_4$ suitable for infrared nonlinear optical applications (IR NLO). $CeBrMoO_4$ and $CeBrWO_4$ exhibit moderate SHG responses of 0.58× AGS and 0.46× AGS, respectively, which are both type-I phase-matching materials. Moderate SHG response, easy-growth of crystals, high ambient stability, and type-I phase-matching behavior set $CeBrMoO_4$ and $CeBrWO_4$ as great materials for IR NLO applications. $CeHaVIO_4$ films also exhibited good

photocurrent response upon light radiation. This work demonstrates the rich structure chemistry of the $REHaVIO_4$ (RE=Y, La-Lu, Ha=Cl, Br; VI=Mo, W) family and the potential presence of more multifunctional materials.

Introduction

Infrared nonlinear optical (IR NLO) materials have been vigorously studied due to their irreplaceable roles in solid-state lasers, which are utilized to expand infrared laser frequency via the second harmonic generation process [1-14]. The options for IR NLO materials are still limited to a few commercial materials such as $ZnGeP_2$, $AgGaS_2$, and $AgGaSe_2$. These commercial materials cannot be utilized to cover the full spectrum range of 3-25 μm due to intrinsic limitations such as low laser damage thresholds ($AgGaS_2$, and $AgGaSe_2$) [15] and double-photon absorption ($ZnGeP_2$) [16]. A state-of-the-art IR NLO material should crystallize in an acentric structure and, ideally, balance a large second harmonic generation coefficient (SHG, d_{ij} >$AgGaS_2$), moderate birefringence (Δn) for phase matchability, high laser damage threshold (LDT, >$AgGaS_2$), large bandgap for good transmission range (>3.5 eV) and good thermal-, air-, and chemical stability, all of which are nearly impossible for many systems. Balancing these properties to satisfy these criteria is not a simple task due to the fact that many of these parameters are intrinsically correlated [17-29]. For example, in general, a material with a large bandgap should have a high LDT, but the SHG coefficients would be expected to be low. Inversely, small bandgap materials are more likely to have large SHG coefficients, but with the price of sacrificing LDT [17, 21, 29-31]. Hence, finding a chemical system, which meets all criteria, is important and challenging.

Oxyhalides, which constitute two anions of oxygen and halogen, have been emerging as important NLO materials, especially for covering visible or ultraviolet spectrum range, but rarely used for IR NLO applications [32-42]. There are two major reasons for this: first, the presence of metal-oxygen bonds, whose intrinsic vibrations are over the spectrum ranges of 3-5 μm and 8-12 μm, resulting in high optical absorption of desired IR spectrum range; second, the strong ionic metal-halogen interactions, which have tight bonding of valence electrons around anions, generating very large bandgaps [32-42]. A very large bandgap is usually accompanied by a small SHG response. Hence, a good strategy to "push" oxyhalides into the IR spectrum range is necessary. One successful strategy to create good oxyhalide IR NLO materials is to incorporate heavy metals like Pb, such as, $Pb_{17}O_8Cl_{18}$ [43], $Pb_{13}O_6C_{l4}Br_{10}$ [44], $Pb_{18}O_8Cl_{15}I_5$ [45]. Another good method to employ oxyhalides as

IR NLO materials is to add more anions such as $[Ba_2F_2][Ge_2O_3S_2]$ [46]. All these strategies have successfully suppressed the bandgaps of inorganic solids, leading to good transmission over the IR spectrum range while maintaining high SHG responses. In this work, we attempted a new strategy of utilizing Ce's partially occupied 4*f* orbitals to narrow the bandgaps of oxyhalides $CeHaVIO_4$ into the IR spectrum range and succeeded. For instance, $CeBrWO_4$ is isostructural to $LaBrWO_4$. By replacing La by Ce, the bandgap was narrowed from 4.2(1) eV to 2.8(1) eV for $LaBrWO_4$ and $CeBrWO_4$, respectively. The synthesis, crystal and electronic structures, and linear and nonlinear optical properties of oxyhalides $CeHaVIO_4$ (Ha=Cl, Br; VI=Mo, W) are reported in this work. $CeBrMoO_4$ is found to be a good IR NLO material with balanced properties (E_g=3.0(1) eV, SHG: 0.58× AGS). Therefore, this work finds a new method to modulate oxyhalides as potential IR NLO materials.

Experimental Details

Synthesis and crystal growth: Raw reactants in this work were used as received without further processing: $CeBr_3$ (Thermo Fisher Scientific, 99.9%), $CeCl_3$ (Thermo Fisher Scientific, 99.9%), Ce_2O_3 (MSE Supplies, 99.9%), MoO_3 (Alfa Aesar, 99.5 %), WO_3 (Alfa Aesar, 99.8%), NaBr (Thermo Fisher Scientific, 99+%), NaCl (Sigma-Aldrich, anhydrous, 99.5%). All these reactants were stored in an argon-filled glovebox and the moisture and oxygen levels of the glovebox were kept below 0.5 ppm.

$CeClVIO_4$ (VI=Mo, W): Flux $CeCl_3$/NaCl was utilized to grow crystals of $CeClVIO_4$ (VI=Mo, W). 0.4 g of $CeCl_3$, Ce_2O_3, and VIO_3 (VI=Mo, W) mixed in a molar ratio of 1:1:3 were loaded into a carbonized silica tube first. Then, 0.4 g of flux of $CeCl_3$/NaCl mixed in a molar ratio of 1:2 were loaded to cover the top of reactants. The silica tubes were transferred out of glovebox and sealed by a torch under a vacuum of 10^{-2} Torr. The tube was heated from room temperature to 820 °C in 10 hrs and held for 168 hrs before naturally cooling down. The crystals were collected after the flux was removed by DI water. **$CeBrVIO_4$ (VI=Mo, W):** A similar synthetic routine was employed with $CeBr_3$/NaBr=1:2 as flux. 0.4 g reactants of $CeBr_3$, Ce_2O_3, and VIO_3 (VI=Mo, W) mixed in a molar ratio of 1:1:3 were covered by 0.4 g flux. The temperature profile of $CeBrVIO_4$ (VI=Mo, W) was identical to $CeClVIO_4$ (VI=Mo, W). The crystals were collected after the flux was washed away by DI water. The optical microscope photos of crystals of $CeHaVIO_4$ (Ha=Cl, Br; VI=Mo, W) are shown in **Figure S1.** All samples in this work are stable in air for a long time.

The mixed-cation compounds of $(La_{0.5}Ce_{0.5})$ $HaVIO_4$ (Ha=Cl, Br; VI=Mo, W) were grown by using the following equations: $3(La_{0.5}Ce_{0.5})HaVIO_4=0.5LaHa_3+0.5CeHa_3+0.5Ce_2O_3+0.5La_2O_3+3VIO_3$ with flux of $CeHa_3/LaHa_3/NaHa=0.5:0.5:2$, where Ha=Cl, Br and VI=Mo, W. The temperature profile of mixed-cation compounds was the same as the pristine compounds.

Single Crystal X-ray Diffraction: Crystals of $CeHaVIO_4$ (Ha=Cl, Br; VI=Mo, W) were manually picked up under an optical microscope and mounted to the Rigaku XtaLAB Synergy-I instrument. The data collection was performed at 290 (5) K. The data collection and integration were done by CrysAlis^{Pro} Software (Agilent Technologies, XRD Products; CrysAlis Pro; Agilent Technologies, Inc). The structural solution and refinement were done with Jana2006 [47]. Details of the data collection and structure refinement are provided in **Table 1**. Atomic coordinates and selected bond distances are listed in **Tables S1** and **S2**. Crystallographic data for $CeHaVIO_4$ (Ha=Cl, Br; VI=Mo, W) have been deposited to the Cambridge Crystallographic Data Centre, CCDC, 12 Union Road, Cambridge CB21EZ, UK. Copies of the data can be obtained free of charge by quoting the depository numbers CCDC- 2302882 ($CeClMoO_4$), CCDC- 2302884 ($CeClWO_4$), CCDC-2302881 ($CeBrMoO_4$), and CCDC- 2302883 ($CeBrWO_4$) .

Lab powder X-ray Diffraction: Powder X-ray diffraction data were collected at room temperature using a Rigaku Mini Flex 6G diffractometer with Cu-Kα radiation (λ =1.5406 Å) in the range $2\theta = 10° – 80°$, at a scan step of 0.04° with ten seconds exposure time.

UV-Vis Measurements: Diffuse-reflectance spectra were recorded at room temperature by a PERSEE-T8DCS UV-Vis spectrophotometer equipped with an integration sphere in the wavelength range of 230−850 nm. The reflectance data, R, were recorded and converted to the Kubelka-Munk function, $f(R)=(1-R)^2(2R)^{-1}$. Tauc plots, $(KM*E)^2$ and $(KM*E)^{1/2}$, were applied to estimate direct and indirect bandgaps, respectively.

Second Harmonic Generation Measurements: Using the Kurtz and Perry method,[48] powder SHG responses of $CeHaVIO_4$ (Ha=Cl, Br; VI=Mo, W) compounds were investigated by a Q-switch laser (2.09 μm, 3 Hz, 50 ns) with various particle sizes, including 38.5–54, 54–88, 88–105, 105–150, and 150–200 μm.. Polycrystalline lab-synthesized $AgGaS_2$ (AGS) was also sieved into similar particle sizes for SHG efficiency comparison. A short pass filter was placed in front of the photomultiplier tube to prevent scattered 1064 nm photons from being detected.

Table 1. Refined crystallographic parameters of $CeClMoO_4$, $CeClWO_4$, $CeBrMoO_4$, and $CeBrWO_4$ from single crystal X-ray diffraction.

Compound	**$CeClMoO_4$**	**$CeClWO_4$**	**$CeBrMoO_4$**	**$CeBrWO_4$**
Formula weight	335.5	423.4	380	467.9
Crystal color	translucent light orange	translucent light yellow	translucent yellow	translucent orange
Temperature (K)	296.97	297.6(7)	296.36	296.4
Radiation, wavelength	Mo-Ka, 0.71073 Å			
Crystal system	Monoclinic			
Space group	*P*1*c*1 (No. 7)			
a(Å)	9.55135(6)	19.6059(2)	9.77746(9)	9.87827(7)
b(Å)	5.79301(5)	5.89450(10)	5.82090(5)	5.92232(3)
c(Å)	7.94951(9)	7.80090(10)	8.03217(7)	7.93937(5)
β (°)	90.0140(7)	101.4746(8)	90.0106(7)	90.0083(6)
V ($Å^3$)	439.851(7)	883.51(2)	457.143(11)	464.473(11)
Z	4	8	4	4
D_c (g cm^{-1})	5.0665	6.3665	5.5207	6.6907
μ (mm^{-1})	13.557	36.679	21.201	42.913
F(000)	596	1448	668	796
Flack Parameter	0.292(16)	0.269(12)	0.033(18)	0.266(15)
R_1, wR_2 (all data)	0.0138, 0.0182	0.0229, 0.0294	0.0157, 0.0193	0.0211, 0.0256
R_1, wR_2 (I > 2σ(I))	0.0136, 0.0181	0.0257, 0.0298	0.0157, 0.0194	0.0208, 0.0255

$R_1 = \sum||F_o| - |F_c||/\sum|F_o|$; $wR_2 = [\sum[w(F_o^2 - F_c^2)^2]/\sum[w(F_o^2)^2]]^{1/2}$, and $w = 1/[\sigma^2F_o^2 + (A \cdot P)^2 + B \cdot P]$, $P = (F_o^2 + 2F_c^2)/3$; A and B are weight coefficients.

DFT Calculations: The electronic structures of $CeHaVIO_4$ (Ha=Cl, Br; VI=Mo, W) compounds, including their density of states (DOS) and electronic band structures, were calculated using Vienna Ab-initio Simulation Package.[49-52] The Perdew−Burke−Ernzerhof (PBE) functional within the generalized gradient approximation (GGA) [53] was adopted to calculate the exchange-correlation potential, with an energy cutoff of 400 eV. The numerical integration of the Brillouin

zone was performed using a Monkhorst−Pack k-point sampling.[54] For $CeBrMoO_4$, $CeBrWO_4$, and $CeClMoO_4$, the k-point mesh is 5 × 9 × 7. For $CeClWO_4$, with a larger unit cell, the k-point mesh is 3 × 7 × 5. Pseudopotentials generated with the projector augmented-wave (PAW) method were employed.[55] To treat the highly correlated Ce 4*f* electrons, an on-site repulsion Hubbard parameter, U = 4 eV, was used.[56]

Photocurrent response measurement. Crystals of $CeHaVIO_4$ (Ha=Cl, Br; VI=Mo, W) are very stable in air. Hence, crystals of $CeHaVIO_4$ (Ha=Cl, Br; VI=Mo, W) were manually crushed and grounded in mortar in air. Ethanol was employed to aid in forming suspension solutions. The suspension solution was slowly dropped on the ITO glass to form a uniform film. The uniformness of the prepared films was checked by an optical microscope. The films were dried at 393K under vacuum for 2 hours. The photocurrent performance of the photoanode was evaluated in a traditional three-electrode configuration, consisting of $CeHaVIO_4$ (Ha=Cl, Br; VI=Mo, W) photoanodes as the working electrode, platinum wire as the counter electrode, and Ag/AgCl as the reference electrode. 1M Na_2SO_4 aqueous solution was used as the electrolyte. Linear sweep voltammetry and I-t scans were collected on the electrochemical workstation (Gamry Interface 5000) under illumination of AM 1.5 (1 sun, 100 mW/cm^2) using a solar simulator (Newport).

Results and discussions

Crystal growth and phase purification

Prior to this work, $CeClMoO_4$ [57-59] and $CeBrMoO_4$ [60] were reported. The high temperature solid-state method was employed to grow the crystals of $CeClMoO_4$ [57-59] and $CeBrMoO_4$ [60]. $CeClMoO_4$ [60] was found as a phase-pure sample while significant amounts of impurity existed in $CeBrMoO_4$ [60] samples. The previous work did not address crystal growth. In this work, we employed salt flux pairs of $CeCl_3$/NaCl and $CeBr_3$/NaBr to grow $CeClMoO_4$ and $CeBrMoO_4$, respectively. Millimeter-sized crystals of $CeClMoO_4$ and $CeBrMoO_4$ were collected after salt flux was removed by DI water as shown in **Figure S1**. The phase purity of $CeClMoO_4$ and $CeBrMoO_4$ was verified by PXRD as shown in **Figure S2** and **Figure S3**, respectively. Two new tungsten-contained compounds, $CeClWO_4$ and $CeBrWO_4$, were grown by salt flux as single-phase large crystals (**Figures S1, S4**, and **S5**). A combination of various halides would be a good flux for the crystal growth of oxyhalides [32].

Crystal Structure

$CeHaVIO_4$ (Ha=Cl, Br; VI=Mo, W) belongs to the $REHaVIO_4$ (RE=Y, La-Lu, Ha=Cl, Br; VI=Mo, W) family [57-65], which exhibits abundant structural chemistry (*vide infra*). Two structure types were found within $CeHaVIO_4$ compounds. $CeClMoO_4$ is isostructural to $CeBrMoO_4$ and $CeBrWO_4$. $CeClWO_4$ crystallizes in its own structure type. $CeClMoO_4$ was reported by Dorhout, P.K. et al in 2010, which crystallizes in centrosymmetric monoclinic space group $P2_1/c$ (no. 14) with unit cell parameters of a = 19.1228(18) Å, b = 5.7992(5) Å, and c = 7.9591(7) Å, and β = 90.037(6)° [57]. Our single crystal X-ray diffraction indicated that $CeClMoO_4$ forms in the acentric monoclinic space group Pc (no. 7) with unit cell parameters of a = 9.5513(1) Å, b = 5.793(1) Å, and c = 7.9495(1) Å, and β = 90.014(1)°, which was also verified by SHG measurements (*vide infra*). $CeBrMoO_4$ is isostructural to $CeClMoO_4$, which was confirmed by our experimental results and a previous study [60]. $CeBrWO_4$ is a new compound, which was never reported. Like $CeBrMoO_4$ and $CeClMoO_4$, $CeBrWO_4$ is also isotypic to $LaBrWO_4$ [32] and crystallizes in the acentric monoclinic space group Pc (no.7) with unit cell parameters of a = 9.8783(1) Å, b = 5.9223(1) Å, and c = 7.9394(1) Å, and β = 90.008(1)°.

The β angles of all these structures are very close to 90˚, making them pseudo-orthorhombic. However, orthorhombic symmetry was precluded because we tested orthorhombic space groups and they all result in much higher R-values and significant residual electron peaks and holes. Due to the pseudo-orthorhombic acentric symmetry, the twinning laws for inversion and 180˚ rotation along a-axis were both considered in our structural refinement.

To simplify the discussion, $CeBrWO_4$ is selected to present the structure of $CeBrMoO_4$ and $CeClMoO_4$. The Wyckoff sequence of $CeBrWO_4$ is a^{14} with the Pearson symbol *mP28*. There are two distinct Ce atoms, two distinct W atoms, two distinct Br atoms, and eight distinct O atoms in the asymmetric unit cell of $CeBrWO_4$ with full occupancy. The crystal structure of $CeBrWO_4$ is summarized in **Figures 1a and 1b**. $CeBrWO_4$ forms a three-dimensional (3D) framework, which is constructed by two-dimensional (2D) $[CeBrO_4]^{6-}$ strips and one-dimensional (1D) $[WO_5]$ strands. The 1D $[WO_5]$ strands are constructed by distorted $[WO_5]$ trigonal bipyramids, which connect to each other via apical oxygen atoms and run along the [001] direction. Five oxygen atoms surround central W atoms with four short interactions of 1.755(7) - 1.842(6) Å and one long

interaction of 2.230(5)-2.239(5) Å. Our previous bonding picture study of $LaBrWO_4$ revealed the moderately strong interaction of the elongated W-O interactions of 2.24 Å [32]. The 2D $[CeBrO_4]^{6-}$ strips are built by distorted tetracapped trigonal prisms $[CeO_6Br_3]$, where six oxygen atoms and three bromine atoms surround the central Ce atoms. The Ce-Br interactions fall into the range of 3.1393(16) - 3.257(2) Å, which is similar to many compounds that include Ce-Br interactions such as, $CeBr_3$ (3.108-3.158 Å) [66], $CeBrMoO_4$(3.112-3.227 Å) [60], $Ce_3(SiS_4)_2Br$(3.101-3.328 Å) [67], etc. The Ce-O interactions are within the range of 2.473(8)-2.697(9) Å of $CeBrWO_4$, which are comparable to many oxides such as $K_6Ce_2(SO_4)_6$(2.498-2.648 Å) [68], $CeBrMoO_4$(2.466-2.726 Å) [60], $CeCu_3Co_4O_{12}$ (2.486 Å) [69], $CeMoBO_6$ (2.427-2.619 Å) [70], etc.

$CeClWO_4$ is a new compound, which crystallizes in a new structure type. $CeClWO_4$ adopts a different unit cell: a = 19.6059(2) Å, b = 5.89450(10) Å, and c = 7.80090(10) Å, and β = 101.4746(8)°, which is a 2× supercell structure of the other three title compounds with the transformation matrix being (2 0 ½, 0 1 0, 0 0 1). This can be demonstrated by comparing the (*h*1*l*) reciprocal lattice planes (**Figure S6**). The refined structure is also in the acentric monoclinic *Pc* (no. 7) space group. The details of refinement are included in **Table 1**. The acentric structure nature of $CeClWO_4$ was also verified by second harmonic generation measurements (*vide infra*). Interestingly, our refined unit cell parameters of $CeClWO_4$ are comparable to those of the $P2_1/c$ $CeClMoO_4$ structure reported by Dorhout, except for the β angle (101.5˚ vs 90.0˚). [57] The Wyckoff sequence of $CeClWO_4$ is a^{28} with the Pearson symbol *mP56*. There are four distinct Ce atoms, four distinct W atoms, four distinct Cl atoms, and sixteen distinct O atoms in the asymmetric unit cell of $CeClWO_4$ with full occupancy. The crystal structure of $CeClWO_4$ is exhibited in **Figures 1b** and **1c**. The 3D crystal structure of $CeClWO_4$ is similar to 3D $CeBrWO_4$ with doubling the [100] axis. The 3D framework of $CeClWO_4$ is constructed by 2D $[CeClO_4]^{6-}$ strips and 1D $[WO_5]$ strands. The 2D $[CeClO_4]^{6-}$ strips are made by distorted tetracapped trigonal prisms $[CeO_6Cl_3]$ via sharing vertices and edges. The 1D $[WO_5]$ strands within $CeClWO_4$ are constructed by distorted $[WO_5]$ trigonal bipyramids, which were also found within $CeBrWO_4$. The W-O interactions within $CeClWO_4$ are 1.730(9) Å-2.190(9) Å, which is comparable with W-O interactions of $CeBrWO_4$ (1.755(7) Å - 2.239(5) Å).

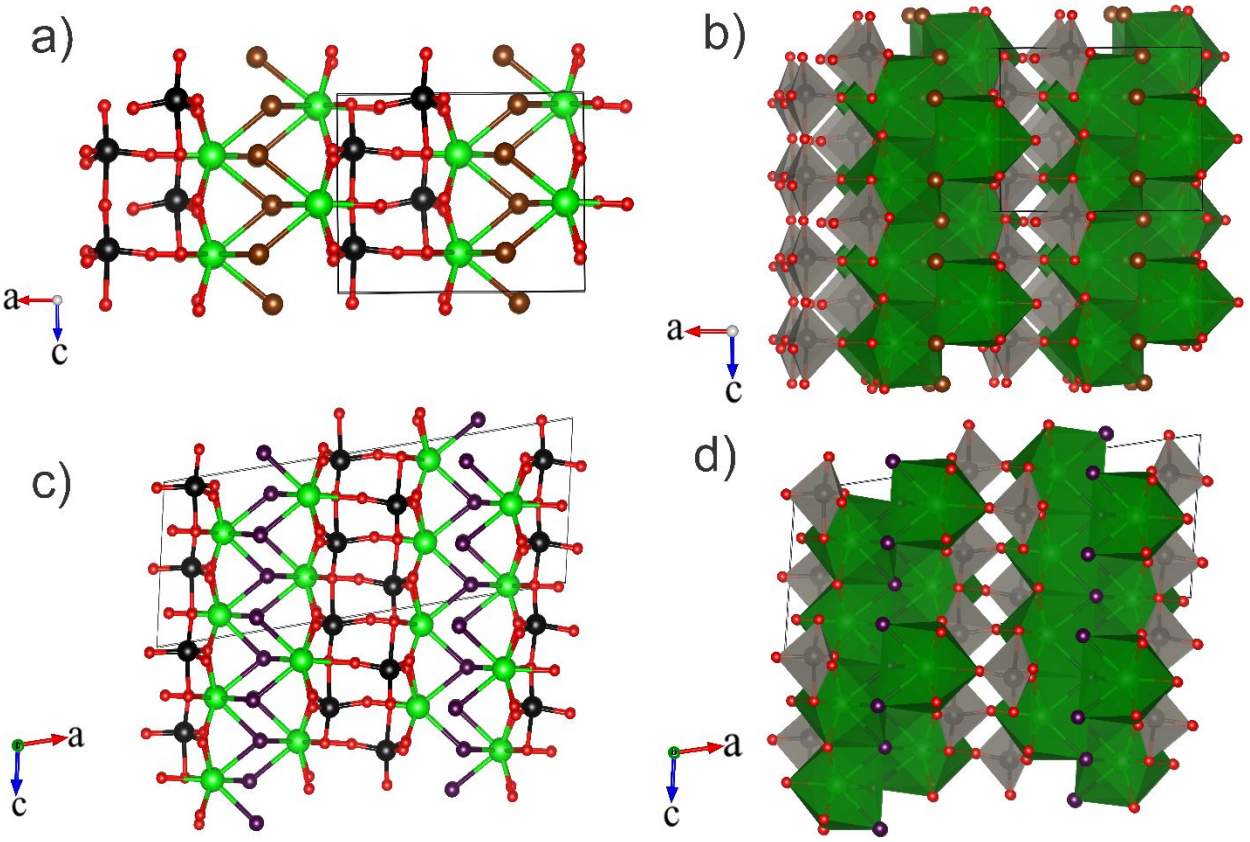

Figure 1. (a) Ball-stick structure and (b) polyhedral structure of $CeBrWO_4$ viewed along the [010] direction. (c) Ball-stick structure and (d) polyhedral structure of $CeClWO_4$ viewed along the [010] direction. Ce: green, W: black, O: red, Br: brown, and Cl: purple.

$REHaVIO_4$ (RE=Y, La-Lu, Ha=Cl, Br; VI=Mo, W) family exhibits very rich structure chemistry. Prior to this work, seven structure types were reported for the $REHaVIO_4$ (RE=Y, La-Lu, Ha=Cl, Br; VI=Mo, W) family, which is summarized in **Table S3** [57-65]. The comparison of physical properties such as magnetic properties, bandgaps, and photoluminescent properties between $CeHaVIO_4$ and the compounds of $REHaVIO_4$ (RE=Y, La-Lu, Ha=Cl, Br; VI=Mo, W) family were summarized in Table S3. This work of $CeClWO_4$ adds the eighth structure type to the $REHaVIO_4$ (RE=Y, La-Lu, Ha=Cl, Br; VI=Mo, W) family. Compared to their differences, these structures exhibit more similarity. 3D framework structure constructed by $[REO_xHa_y]$ polyhedra and $[VIO_z]_{z=4 \text{ or } 5}$ units is a common feature for the $REHaVIO_4$ (RE=Y, La-Lu, Ha=Cl, Br; VI=Mo, W) family. The 1D $[VIO_5]_{VI=Mo \text{ or } W}$ strands were also discovered within $CeClMoO_4$ (space group $P2_1/c$) structure type [57], $LaClWO_4$(space group $Pbc2_1$) structure type [61], and $LaClWO_4$ (space group $Pmcn$) structure type [61]. The discrepancies between structures reported for the same

compound, such as Dorhout's $CeClMoO_4$ in $P2_1/c$ *vs.* this work's $CeClMoO_4$ in *Pc*, is likely due to polymorphism – a given $REHaVIO_4$ compound may adopt similar but different crystal structures, especially when prepared with different synthetic methods. For example, $LaClWO_4$ crystallizes in acentric orthorhombic $Pbc2_1$ and centrosymmetric orthorhombic Pmcn space group [60]. In our own study of $LaHaVIO_4$ and $CeHaVIO_4$, we found crystals whose diffraction patterns indicate much larger unit cells or even exhibit diffused scattering, which suggests the possible intergrowth between different polymorph structures. We are devoting more efforts into these challenging crystals in hope to provide more insights into the abundant structural chemistry in the $REHaVIO_4$ (RE=Y, La-Lu, Ha=Cl, Br; VI=Mo, W) family, which accounts for their broad applications such as photoluminescent applications, [62] NLO applications, [32] and the photocurrent response in this work.

Linear Optical properties

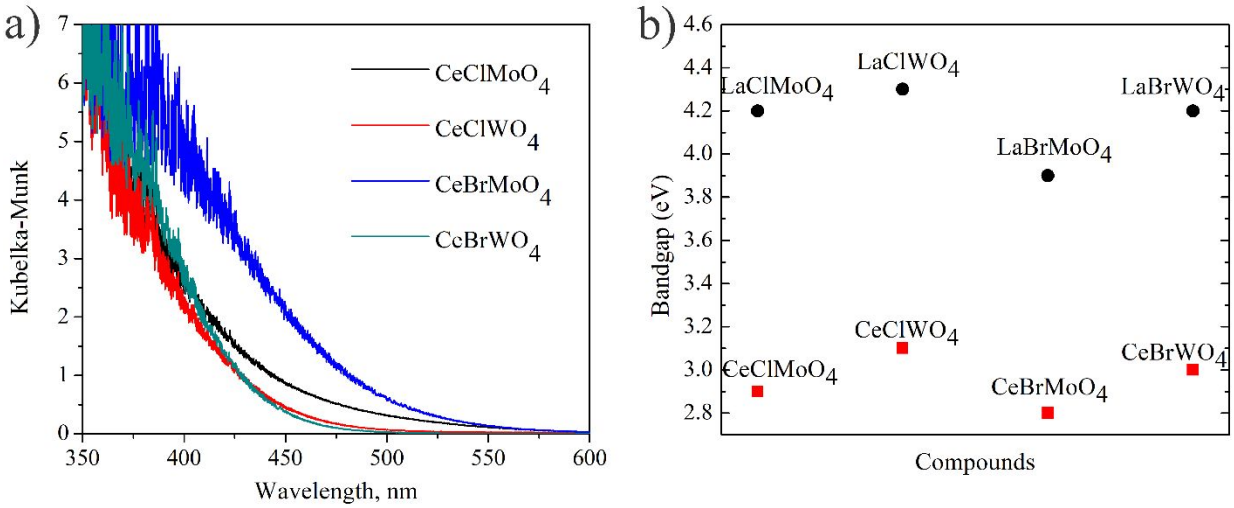

Figure 2. (a) Kubelka-Munk diffuse reflectance solid-state UV-Vis spectra of $CeHaVIO_4$ (Ha=Cl, Br; VI=Mo, W). (b) The comparison of bandgaps between $CeHaVIO_4$ (Ha=Cl, Br; VI=Mo, W) and $LaHaVIO_4$ (Ha=Cl, Br; VI=Mo, W) compounds.

The optical bandgaps of $CeHaVIO_4$ (Ha=Cl, Br; VI=Mo, W) were estimated by UV-Vis spectrum measurements (**Figure 2a**). $CeClWO_4$ is similar to $CeBrWO_4$, which exhibits a transition around 450nm. Based on electronic structure calculation, $CeHaVIO_4$ are direct-bandgap semiconductors (*vide infra*). The direct allowed transitions of $CeHaVIO_4$ were calculated by the Tauc plots, which were shown in **Figure 2b**. The calculated direct bandgap of $CeClWO_4$ and $CeBrWO_4$ are 3.1(1)

eV and 3.0(1) eV, respectively. There is a transition around 500 nm observed for $CeClMoO_4$, which results in the calculated direct bandgap of 2.9(1) eV. The $CeBrMoO_4$ possesses the smallest bandgap of 2.8(1) eV, which originates from its transition around 575 nm. Compared with the isostructural counterparts $LaHaVIO_4$ (Ha=Cl, Br; VI=Mo, W), the bandgaps of $CeHaVIO_4$ compounds are much smaller (**Figure 2b**). The suppression of bandgaps of $CeHaVIO_4$ compounds originate from the partially filled *4f* orbitals of Ce atoms (*vide infra*). The bandgap suppression also agreed well with the physical appearance of crystals of $REHaVIO_4$ (RE=La, Ce; Ha=Cl, Br; VI=Mo, W), where $LaHaVIO_4$ and $CeHaVIO_4$ compounds are colorless and colorful [32], respectively. Tuning the bandgap of inorganic solids is crucial for many applications such as second harmonic generation [25] and photovoltaics [71]. Our attempts to tune the bandgap of $CeHaVIO_4$ via replacing Ce with La was found to be effective. As shown in **Figures S7-S10**, $(La_{0.5}Ce_{0.5})ClMoO_4$, $(La_{0.5}Ce_{0.5})ClWO_4$, $(La_{0.5}Ce_{0.5})BrMoO_4$, and $(La_{0.5}Ce_{0.5})BrWO_4$ were found to be single phase samples. The bandgap of $(La_{0.5}Ce_{0.5})$ $ClMoO_4$, $(La_{0.5}Ce_{0.5})ClWO_4$, $(La_{0.5}Ce_{0.5})BrMoO_4$, and $(La_{0.5}Ce_{0.5})BrWO_4$ were estimated by UV-Vis measurements to be 3.8(1) eV, 3.5(1) eV, 3.6(1) eV, and 3.9(1) eV, respectively. As shown in **Figure S11**, the bandgap of $(La_{0.5}Ce_{0.5})HaVIO_4$ (Ha=Cl, Br; VI=Mo, W) samples reside between $CeHaVIO_4$ and $LaHaVIO_4$ samples. Mixing La and Ce would be a good strategy to tune their bandgaps. The narrowed bandgaps of $CeHaVIO_4$ compounds result in good transmission in the IR range. The infrared spectrum of $CeHaVIO_4$ compounds are shown in **Figures S12** and **S13**. There were no intrinsic vibrational absorption chemical bonds in the wavelength of 2.5–18.2 μm for all $CeHaVIO_4$ compounds. $CeClWO_4$ and $CeBrWO_4$ exhibited comparable IR spectra with three absorption peaks detected around 550 cm^{-1}, which agree well with $LaBrWO_4$ [32]. The strong absorption peaks around 550 cm^{-1} can be assigned to the υ(W-O) vibrations [32]. The IR spectrum of $CeClMoO_4$ is comparable to $CeBrMoO_4$ with two strong absorption peaks detected around 550 $cm^{-1,}$ which originate from the υ(Mo-O) vibrations [32]. A comparable IR spectrum was also found in $LaBrMoO_4$ [32].

Electronic Structures

$LaHaVIO_4$ (Ha=Cl, Br, VI=Mo, W) is isostructural to $CeHaVIO_4$ (Ha=Cl, Br, VI=Mo, W), except $CeClWO_4$. It would be interesting to investigate why there are significant bandgap differences

between them. Hence, we employed DFT calculations to study the electronic structures of $CeHaVIO_4$ (**Figures 3, S14-S18**).

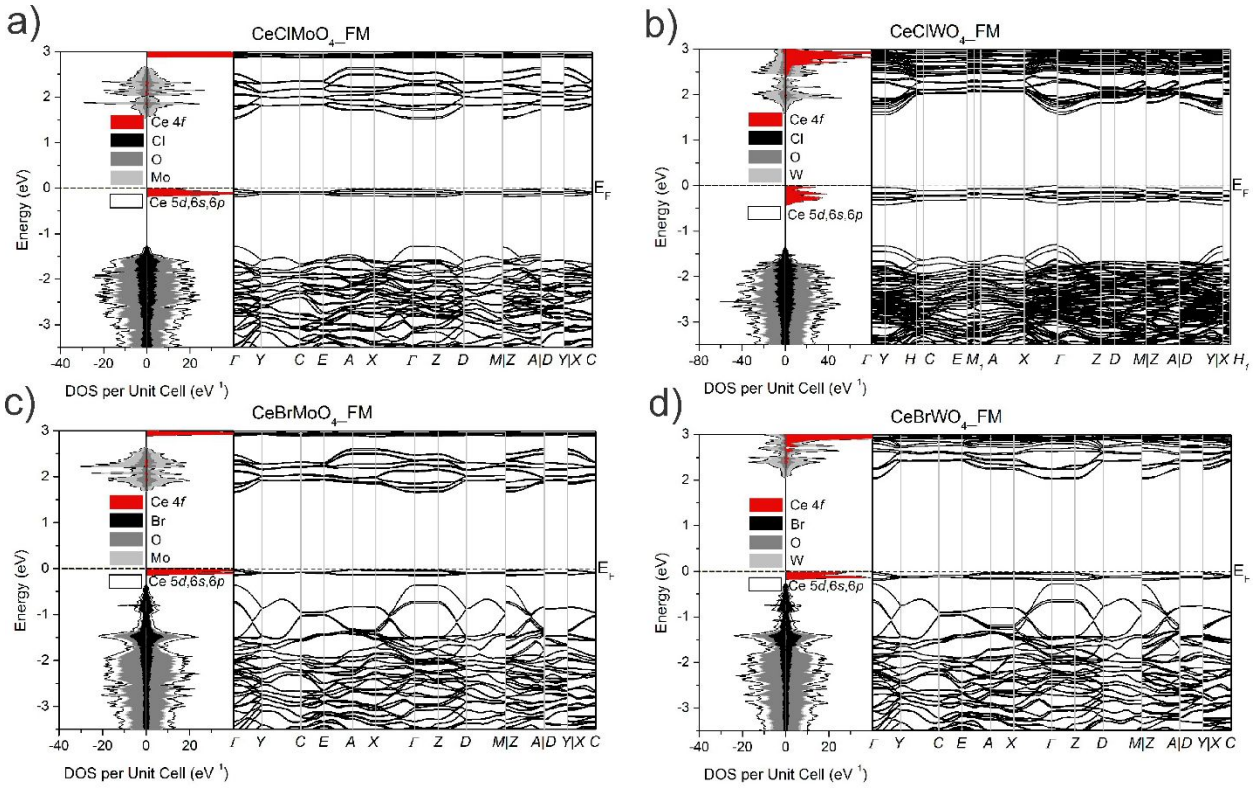

Figure 3. The DOS curves and electronic band structures of $CeHaVIO_4$ (Ha=Cl, Br, VI=Mo, W).

Using the structures from single crystal refinement, we calculated the DOS and electronic band structures of $CeClMoO_4$, $CeClWO_4$, $CeBrMoO_4$, and $CeBrWO_4$. Due to the strong correlation of Ce 4*f* electrons, the Hubbard parameter (U = 4 eV) had to be employed. Otherwise, the self-consistent calculations do not converge. Formally, the valence of Ce is +3, which means each Ce atom has one 4*f* electron and thus 1 μ_B local moment. Because there are multiple Ce atoms in a unit cell, we tried both ferromagnetic and antiferromagnetic ordering of Ce atoms' local moments as well. **Figure 3** lists the DOS and band structures from ferromagnetic calculations of the four compounds. The antiferromagnetic results are shown in **Figure S15-18** in Supporting Information. From both sets of results, we can draw the same conclusions below.

The most prominent feature among all these $CeHaVIO_4$ compounds is their highly localized Ce 4*f* states. They form a narrow peak in the DOS and very flat bands in the band structures. Moreover, it represents the valence band edges in all cases. For comparison, we also calculated the electronic

structure for $LaBrWO_4$, which is also shown in **Figure S14**. La has no 4*f* electron in $LaHaVIO_4$. As a result, the La 4*f* states are absent in DOS and band structure. The valence band edge is mainly contributed by Br states. This comparison clearly explains the band gap differences between $CeHaVIO_4$ and $LaHaVIO_4$ – Ce's 4*f* states significantly reduce the band gap of $CeHaVIO_4$. The calculated bandgaps for $CeHaVIO_4$ (Ha=Cl, Br, VI=Mo, W) are around 2 eV, which are smaller than experimentally estimated values. The underestimation of bandgaps of inorganic solids is common for DFT calculations [72]. DFT calculations confirmed the semiconducting nature of CeHaVIO4, which was also verified by UV-Vis measurements. The charge-balanced formula $(Ce^{3+})(Ha^{-})(VI^{6+})(O^{2-})_4$ can be established by assigning a formal charge of 3+ to the Ce atoms, 6+ to the Mo and W atoms,1- to the Cl and Br atoms, and 2- to the O atoms. Bond valence sum calculations found the BVS of Ce atoms and W atoms to be 2.98 and 5.95 receptivity for $CeClWO_4$, which suggests Ce atoms and W atoms with oxidation 3+ and 6+, respectively [24].

Nonlinear Optical properties

The nonlinear optical properties of $CeHaVIO_4$ (Ha=Cl, Br, VI=Mo, W) were measured and presented in **Figure 4.** All samples exhibited SHG response under 2090 nm incident lasers, which confirmed the acentric nature of $CeHaVIO_4$ samples. $CeBrMoO_4$ and $CeBrWO_4$ own comparable SHG responses of 0.58× AGS and 0.46× AGS, respectively for samples of 225 μm particle. The SHG intensity of $CeBrMoO_4$ and $CeBrWO_4$ increases with increasing particle size, which indicates that $CeBrMoO_4$ and $CeBrWO_4$ are type-I phase-matching materials. $CeClWO_4$ exhibited a much lower SHG response of 0.22× AGS for a sample of 225 μm particle. $CeClMoO_4$ possessed the lowest SHG response of 0.06× AGS for samples of 225 μm particle. $CeClMoO_4$ and $CeClWO_4$ are not type-I phase-matching materials, and the SHG intensity of $CeBrMoO_4$ and $CeBrWO_4$ decreases as the particle size increases (**Figure 4**). The isostructural nature and comparable bandgaps between $CeBrMoO_4$, $CeBrWO_4$, and $CeClMoO_4$ result in distinct SHG responses. $CeClMoO_4$ and $CeClWO_4$ are non-phase-matching materials compared to $CeBrMoO_4$ and $CeBrWO_4$. Many factors such as the crystal quality or different crystal structures would significantly affect NLO properties [73]. The future planned study will be focused on measurements of the birefringence of $CeHaVIO_4$ to understand this difference. The higher degree distortion of 1D $[VIO_5]_{VI=Mo\ or\ W}$ strands plays an important role in enhancing SHG within $CeBrMoO_4$ and CeBrWO4, which was also observed for $LaBrWO_4$ compared to $LaBrMoO_4$ [32].

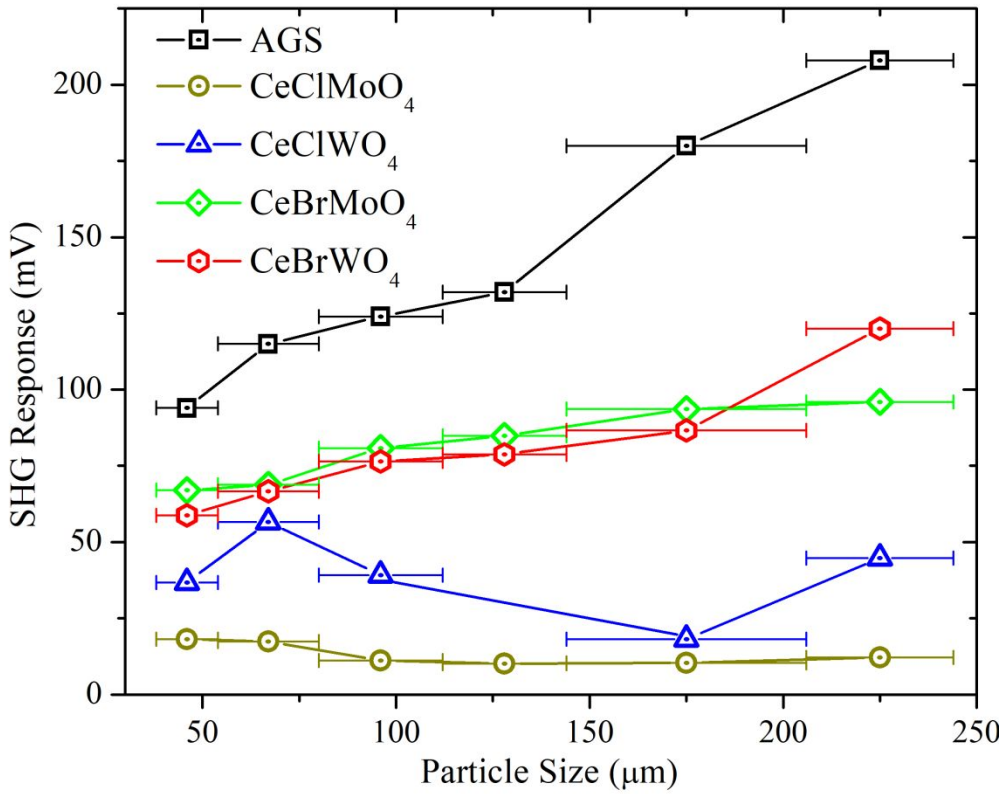

Figure 4. Size-dependent SHG intensities of $CeHaVIO_4$ (Ha=Cl, Br, VI=Mo, W) samples and the $AgGaS_2$ (AGS) reference.

Photocurrent response

The bandgaps of $CeHaVIO_4$ fall into the range of 2.8(1)-3.1(1) eV, which originates from the presence of partially filled 4*f* orbitals of cerium. These partially filled 4*f* orbitals populate between the valance band and conduction band. $CeHaVIO_4$ crystals can absorb visible light due to their small bandgap nature (**Figure 2a**). The capability of absorption of visible lights coupled with excellent ambient stability contributed to us exploring the photocurrent response of $CeHaVIO_4$ samples. A material that can generate high photocurrent density under light radiation can be used for photovoltaics to reduce our dependence on fossil energy [24, 28]. The photocurrent response of $CeHaVIO_4$ samples are presented in **Figure 5**. As shown in **Figure 5**, $CeHaVIO_4$ samples exhibit good photocurrent response. The reproducibility of the photocurrent response of $CeHaVIO_4$ samples were tested by measuring three samples of each specimen, which are summarized in **Figures S19-S22**. All $CeHaVIO_4$ samples exhibited good reproducibility. $CeClMoO_4$ and $CeClWO_4$ exhibited comparable photocurrent responses of 332 nA Cm^{-2} and 369 nA Cm^{-2},

respectively. The photocurrent density of $CeBrMoO_4$ was 263 nA Cm^{-2}. $CeBrWO_4$ possessed the lowest photocurrent response of 138 nA Cm^{-2}. The photocurrents of $CeHaVIO_4$ samples slightly decrease after a few cycles, which was observed in many photocurrent-responding materials and originates from the photocorrosion of photoanodes [24, 28]. A comparison of photocurrent response among $CeHaVIO_4$ and many previously reported sulfides and oxyhalides are tabulated in **Table S4** [74-89]. $CeHaVIO_4$ exhibit comparable or better photocurrent response than many compounds such as $Eu_3Gd_6MgS_2B_{20}O_{41}$ (0.12 μA/cm^2) [78], $Sr_6Cd_2Sb_6S_{10}O_7$ (0.065μA/cm^2) [77], $BaCuSbS_3$ (0.055 μA/cm^2) [76], $BaCuSbSe_3$ (0.03μA/cm^2) [76], $RbIn_4S_6Cl$ (0.029μA/cm^2) [75], $Pb_5Sn_3S_{10}Cl_2$ (0.019μA/cm^2) [75], $Rb_2Ba_3Cu_2Sb_2S_{10}$ (0.006μA/cm^2) [74]. Photocurrent measurements can be useful to extract more intrinsic properties of inorganic solids. An external quantum efficiency (EQE) measurement can be employed to determine the bandgaps of $CeHaVIO_4$ [90], which are undergoing. $CeHaVIO_4$ system exhibits both good NLO properties and photocurrent response, which indicates that they are good multifunctional materials. There might exist more new compounds in the $REHaVIO_4$(RE=La-Lu, Ha=Cl, Br, VI=Mo, W) system, which may uncover more multifunctional materials. The discovery of new heteroanionic compounds usually results in exciting physical properties such as recent works of $C(NH_2)_3BF_4$ [91] and $Ca_2B_3O_6X$ (X = Cl and Br) [92].

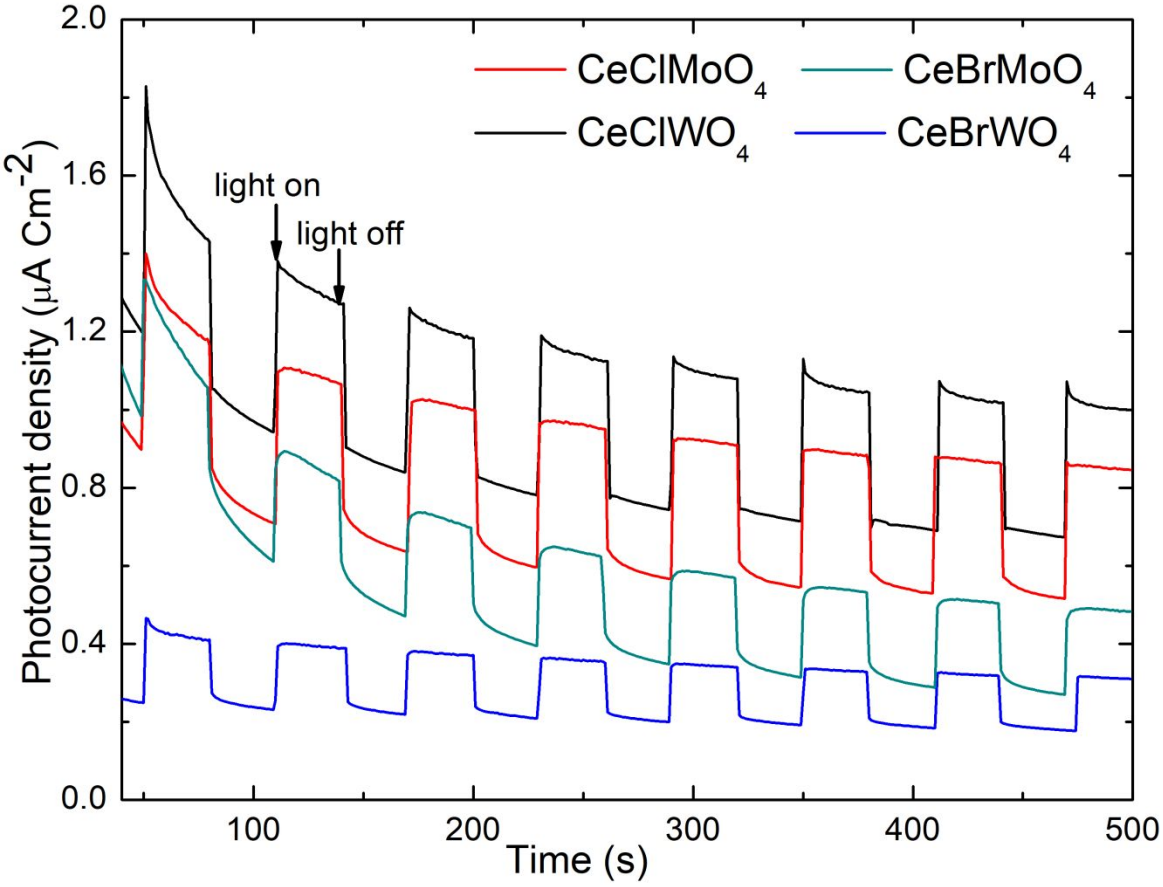

Figure 5. Photocurrent density of $CeHaVIO_4$ (Ha=Cl, Br, VI=Mo, W) photoanodes over time.

Conclusions

Millimeter-sized crystals of four heteroanionic oxyhalides, $CeClMoO_4$, $CeBrMoO_4$, $CeClWO_4$, and $CeBrWO_4$, had been grown by a halide salt flux method, which are stable in ambient air for a long time. $CeClMoO_4$, $CeBrMoO_4$, $CeClWO_4$, and $CeBrWO_4$ were studied as multifunctional materials, which combine good second harmonic generation (SHG) response and photocurrent signals. Two structure types were found for the $CeHaVIO_4$ (Ha=Cl, Br, VI=Mo, W) system. $CeClMoO_4$ is isostructural to $CeBrMoO_4$ and $CeBrWO_4$, which forms in the $LaBrMoO_4$ structure type. $CeClWO_4$ crystallizes in a new structure type, which adds the eighth structure type to the $REHaVIO_4$ (RE=Y, La-Lu, Ha=Cl, Br; VI=Mo, W) family. The $CeHaVIO_4$ system features a 3D framework, which is made by 2D $[REHaO_4]^{6-}$ strips and 1D $[VIO_5]$ strands. Compared with isostructural $LaHaVIO_4$ system, the bandgaps of $CeHaVIO_4$ system are significantly suppressed from 3.9(1)-4.3(1) eV to 2.8(1)-3.1(1) eV, respectively. The presence of partially filled *4f* orbitals

of cerium atoms accounts for the narrower bandgaps of $CeHaVIO_4$. The $CeHaVIO_4$ system all exhibited SHG responses. $CeBrMoO_4$ and $CeBrWO_4$ are both type-I phase-matching materials, which possess moderate SHG response of 0.58× and 0.46× AGS, respectively. $CeBrMoO_4$ and $CeBrWO_4$ are good candidates for IR NLO application due to their moderate SHG response, easy-growth of crystals, high ambient stability, and type-I phase-matching behavior. $CeHaVIO_4$ films can also generate photocurrent response in the range of 138 nA Cm^{-2}- 369 nA Cm^{-2} upon light radiation. The $REHaVIO_4$ (RE=Y, La-Lu, Ha=Cl, Br; VI=Mo, W) family owns rich structural chemistry, which has eight structure types. Functionalities such as NLO application, photoluminescent response, and photocurrent response were found within the $REHaVIO_4$ family, where more multifunctional materials can be grown by halide salt flux methods.

ASSOCIATED CONTENTS

Supporting Information

The refined crystallographic data, crystal structure summary of the $REHaVIO_4$ (Ha=Cl, Br; RE= La-Lu; VI=Mo, W) system, comparison of photocurrent density, microscope photos of crystals, lab powder X-ray diffraction results, the (h1l) planes, IR spectrum, DOS plots, photocurrent density results.

Acknowledgments

This research was supported by the National Science Foundation (DMR-2316811). F. W acknowledges NSF MRI 2117129 for funding the single crystal X-ray diffractometer. W. W thanks the support by U.S. Department of Energy's Office of Energy Efficiency and Renewable Energy (EERE) under the Solar Energy Technologies Office Award Number DE-EE0009525. The views expressed herein do not necessarily represent the views of the U.S. Department of Energy or the United States Government. Z. J thanks Yangjinyi Wang's help on plotting TOC figure.

Corresponding author

Fei Wang FeiWang@MissouriState.edu

Jian Wang jian.wang@wichita.edu

Notes

The authors declare no competing financial interest.

References

[1]. Abudurusuli, J. Li and S. Pan, *Dalton Trans.*, 2021, **50**, 3155–3160.
[2]. D. F. Eaton, *Science*, 1991, **253**, 281–287.
[3]. K. Wu and S. Pan, *Coord. Chem. Rev.*, 2018, **377**, 191–208.
[4]. P. S. Halasyamani and K. R. Poeppelmeier, *Chem. Mater.*, 1998, **10**, 2753–2769.
[5]. H. Yu, M. L. Nisbet and K. R. Poeppelmeier, *J. Am. Chem. Soc.*, 2018, **140**, 8868–8876.
[6]. H. Yu, W. Zhang, J. Young, J. M. Rondinelli and P. S. Halasyamani, *Adv. Mater.*, 2015, **27**, 7380–7385
[7]. H.-M. Zhou, L. Xiong, L. Chen and L.-M. Wu, *Angew. Chem. Int. Ed Engl.*, 2019, **58**, 9979–9983.
[8]. F.-F. Mao, C.-L. Hu, X. Xu, D. Yan, B.-P. Yang and J.-G. Mao, *Angew. Chem. Int. Ed Engl.*, 2017, **56**, 2151–2155.
[9]. C. Wu, T. Wu, X. Jiang, Z. Wang, H. Sha, L. Lin, Z. Lin, Z. Huang, X. Long, M. G. Humphrey and C. Zhang, *J. Am. Chem. Soc.*, 2021, **143**, 4138–4142.
[10]. D. Mei, J. Jiang, F. Liang, S. Zhang, Y. Wu, C. Sun, D. Xue and Z. Lin, *J. Mater. Chem. C Mater. Opt. Electron. Devices*, 2018, **6**, 2684–2689.
[11]. S.-F. Li, X.-M. Jiang, Y.-H. Fan, B.-W. Liu, H.-Y. Zeng and G.-C. Guo, *Chem. Sci.*, 2018, **9**, 5700–5708.
[12]. B.-W. Liu, H.-Y. Zeng, X.-M. Jiang and G.-C. Guo, *CCS Chem.*, 2020, 964–973.
[13]. C. Wang, S. Xiao, X. Xiao, H. Zhu, L. Zhou, Y. Wang, X. Du, Y. Wang, Z. Yang, R. Duan, M. Zhong, H.-G. Rubahn, G. Zhang, Y. Li and J. He, *J. Phys. Chem. C Nanomater. Interfaces*, 2021, **125**, 15441–15447.
[14]. B.-W. Liu, X.-M. Jiang, H.-Y. Zeng and G.-C. Guo, *J. Am. Chem. Soc.*, 2020, **142**, 10641–10645.
[15]. A. Abudurusuli, J. Huang, P. Wang, Z. Yang, S. Pan and J. Li, *Angew. Chem. Int. Ed Engl.*, 2021, **60**, 24131–24136.
[16] R. He, Z. S. Lin, T. Zheng, H. Huang and C. T. Chen, *J. Phys. Condens. Matter*, 2012, **24**, 145503.
[17] B. Ji, F. Wang, K. Wu, B. Zhang and J. Wang, *Inorg. Chem.*, 2023, **62**, 574–582.
[18] C. Cropek, V. Nguyen, S. K. Chhetri, J. Hu, S. Guo and J. Wang, *Crystals (Basel)*, 2022, **12**, 1505.

[19] S. Bardelli, Z. Ye, F. Wang, B. Zhang and J. Wang, *Z. Anorg. Allg. Chem.*, 2022, **648**, e202100388.

[20] B. Ji, A. Sarkar, K. Wu, A. Swindle and J. Wang, *Dalton Trans.*, 2022, **51**, 4522–4531.

[21] V. Nguyen, B. Ji, K. Wu, B. Zhang and J. Wang, *Chem. Sci.*, 2022, **13**, 2640–2648.

[22] B. Ji, K. Wu, Y. Chen, F. Wang, A. J. Rossini, B. Zhang and J. Wang, *Inorg. Chem.*, 2022, **61**, 2640–2651.

[23] Z. Ye, S. Bardelli, K. Wu, A. Sarkar, A. Swindle and J. Wang, *Z. Anorg. Allg. Chem.*, 2022, **648**, e202100271.

[24] B. Ji, E. Guderjahn, K. Wu, T. H. Syed, W. Wei, B. Zhang and J. Wang, *Phys. Chem. Chem. Phys.*, 2021, **23**, 23696–23702.

[25] G. Cicirello, K. Wu, B. B. Zhang and J. Wang, *Inorg. Chem. Front.*, 2021, **8**, 4914–4923.

[26] B. Ji, K. Pandey, C. P. Harmer, F. Wang, K. Wu, J. Hu and J. Wang, *Inorg. Chem.*, 2021, **60**, 10603–10613.

[27] G. Cicirello, K. Wu and J. Wang, *J. Solid State Chem.*, 2021, **300**, 122226.

[28] C. Cropek, B. Ji, A. Sarkar, F. Wang, T. H. Syed, W. Wei, S.-P. Guo and J. Wang, *CrystEngComm*, 2023, **25**, 1175–1185.

[29] S.-F. Li, X.-M. Jiang, Y.-H. Fan, B.-W. Liu, H.-Y. Zeng and G.-C. Guo, *Chem. Sci.*, 2018, **9**, 5700–5708.

[30] Z. Li, J. Yao and Y. Wu, *Cryst. Growth Des.*, 2020, **20**, 7550–7564.

[31] X. Chen and K. M. Ok, *Chem. Asian J.*, 2020, **15**, 3709–3716.

[32] Z. Jiao, O. M. Mireles, K. Ensz, F. Wang, M. Liang, P. S. Halasyamani, B. Zhang, D. P. Rillema and J. Wang, *Chem. Mater.*, 2023, **35**, 6998–7010.
[33] M. Cheng, W. Jin, Z. Yang and S. Pan, *Inorg. Chem.*, 2020, **59**, 13014–13018.
[34] S. Han, M. Mutailipu, A. Tudi, Z. Yang and S. Pan, *Chem. Mater.*, 2020, **32**, 2172–2179
[35] H. Li, H. Wu, X. Su, H. Yu, S. Pan, Z. Yang, Y. Lu, J. Han and K. R. Poeppelmeier, *J. Mater. Chem. C Mater. Opt. Electron. Devices*, 2014, **2**, 1704.
[36] W. Zhao, S. Pan, J. Han, Z. Zhou, X. Tian and J. Li, *Inorg. Chem. Commun.*, 2011, **14**, 566–568.
[37] W. Jeitschko, T. A. Bither and P. E. Bierstedt, *Acta Crystallogr. B*, 1977, **33**, 2767–2775.
[38] C. Funk, O. Reckeweg, F. J. DiSalvo, A. Schulz, S. Klenner, R. Pöttgen, O. Janka and T. Schleid, *J. Alloys Compd.*, 2020, **844**, 156038.
[39] J. Zhou, Y. Liu, H. Wu, H. Yu, Z. Lin, Z. Hu, J. Wang and Y. Wu, *Angew. Chem. Int. Ed Engl.*, 2020, **59**, 19006–19010.
[40] W. Zhang, Z. Wei, Z. Yang and S. Pan, *Inorg. Chem.*, 2019, **58**, 13411–13417.
[41] J. Guo, S. Cheng, S. Han, Z. Yang and S. Pan, *Adv. Opt. Mater.*, 2021, **9**, 2001734.
[42] X. Chen, H. Jo and K. M. Ok, *Angew. Chem. Int. Ed Engl.*, 2020, **59**, 7514–7520.
[43]. H. Zhang, M. Zhang, S. Pan, X. Dong, Z. Yang, X. Hou, Z. Wang, K. B. Chang and K. R. Poeppelmeier, *J. Am. Chem. Soc.,* 2015, **137**, 8360–8363.

[44]. X. Chen, H. Jo and K. M. Ok, *Angew. Chem. Int. Ed Engl.,* 2020, **59**, 7274–7274.

[45]. X. Chen, Q. Jing and K. M. Ok, *Angew. Chem. Int. Ed Engl.,* 2020, **59**, 20323–20327.

[46]. H. Liu, Z. Song, H. Wu, Z. Hu, J. Wang, Y. Wu and H. Yu, *ACS Mater. Lett.,* 2022, **4**, 1593–1598.

[47] V. Petříček, M. Dušek and L. Palatinus, *Z. Kristallogr. Cryst. Mater.*, 2014, **229**, 345–352
[48] S. K. Kurtz and T. T. Perry, *J. Appl. Phys.*, 1968, **39**, 3798–3813.
[49] G. Kresse and J. Hafner. *Phys. Rev. B: Condens. Matter Mater. Phys.* 1993, **47**, 558– 561.
[50] G. Kresse and J. Hafner. *Phys. Rev. B: Condens. Matter Mater. Phys.* 1994, **49,** 14251–14269.

[51] G. Kresse and J. Furthmüller. *Comput. Mater. Sci.* 1996, **6**, 15– 50.

[52] G. Kresse and J. Furthmüller. *Phys. Rev. B: Condens. Matter Mater. Phys.* 1996, **54**, 11169–11186.

[53] J. P. Perdew, K. Burke and M. Ernzerhof. *Phys. Rev. Lett.* 1996, **77**, 3865– 3868.

[54] H. J. Monkhorst and J. D. Pack. *Phys. Rev. B: Condens. Matter Mater. Phys.* 1976, **13**, 5188– 5192.

[55] G. Kresse and D. Joubert. *Phys. Rev. B: Condens. Matter Mater. Phys*. 1999, **59**, 1758–1775.

[56] S. L. Dudarev and G.A. Botton, S. Y. Savrasov, C. J. Humphreys and A. P. Sutton. *Phys. Rev. B: Condens. Matter Mater. Phys.* 1998, **57**, 1505– 1509.

[57] I. Hartenbach, T. Schleid, S. Strobel and P. K. Dorhout, *Z. Anorg. Allg. Chem.*, 2010, **636**, 1183–1189.
[58] T. Schleid and I. Hartenbach, *Z. Anorg. Allg. Chem.*, 2009, **635**, 1904–1909.
[59] I. Hartenbach, S. Strobel, T. Schleid, K. W. Krämer and P. K. Dorhout, *Z. Anorg. Allg. Chem.*, 2009, **635**, 966–975.
[60] I. Hartenbach, H. Henning, T. Schleid, T. Schustereit and S. Strobel, *Z. Anorg. Allg. Chem.*, 2013, **639**, 347–353.
[61] L. H. Brixner, H. Y. Chen and C. M. Foris, *J. Solid State Chem.*, 1982, **45**, 80–87.
[62] T. Schleid and I. Hartenbach, *Z. Kristallogr. Cryst. Mater.*, 2016, **231**, 449–466.
[63] T. Schustereit, T. Schleid, H. A. Höppe, K. Kazmierczak and I. Hartenbach, *J. Solid State Chem.*, 2015, **226**, 299–306.
[64] T. Schustereit, H. Henning, T. Schleid and I. Hartenbach, *Z. Naturforsch. B J. Chem. Sci.*, 2013, **68**, 616–624.
[65] T. Schustereit, T. Schleid and I. Hartenbach, *Solid State Sci.*, 2015, **48**, 218–224.
[66]. W. H. Zachariasen, *Acta Crystallogr.,* 1948, **1**, 265–268.

[67]. R. Riccardi, D. Gout, G. Gauthier, F. Guillen, S. Jobic, A. Garcia, D. Huguenin, P. Macaudière, C. Fouassier and R. Brec, *J. Solid State Chem.,* 1999, **147**, 259–268.

[68]. V. Y. Kuznetsov, L. M. Dikareva, D. L. Rogachev and M. A. Porai-Koshits, *J. Struct. Chem.,* 1986, **27**, 165–168.

[69]. I. Yamada, T. Odake, A. Tanaka, Y. Okazaki, F. Toda, Y. Ishii, T. Taniguchi, S. Kawaguchi and A. Hariki, *Inorg. Chem.,* 2020, **59**, 8699–8706.

[70]. D. Zhao, W.-D. Cheng, H. Zhang, S.-P. Hang and M. Fang, *Dalton Trans.,* 2008, 3709-3714.

[71] M. J. Wu, C. C. Kuo, L. S. Jhuang, P. H. Chen, Y. F. Lai and F. C. Chen, *Adv. Energy Mater.*, 2019, **9**, 1901863.

[72] G. Cicirello, M. Wang, Q. P. Sam, J. L. Hart, N. L. Williams, H. Yin, J. J. Cha, J. Wang. *J. Am. Chem. Soc.* 2023, **145**, 14, 8218–8230.

[73] D.J. Clark, J.-H. Zhang, A.J. Craig, A. Weiland, J.A. Brant, J.B. Cho, Y.S. Kim, J. I. Jang and J. A. Aitken *J. Alloys Compd.* 2022, **917**, 165381.

[74] C. Liu, Y. Xiao, H. Wang, W. Chai, X. Liu, D. Yan, H. Lin and Y. Liu, *Inorg. Chem.*, 2020, **59**, 1577–1581.
[75] L.-T. Jiang, M.-Z. Li, X.-M. Jiang, B.-W. Liu and G.-C. Guo, *Dalton Trans.*, 2022, **51**, 6638–6645.
[76] C. Liu, P. Hou, W. Chai, J. Tian, X. Zheng, Y. Shen, M. Zhi, C. Zhou and Y. Liu, *J. Alloys Compd.*, 2016, **679**, 420–425.
[77] S. Al Bacha, S. Saitzek, E. E. McCabe and H. Kabbour, *Inorg. Chem.*, 2022, **61**, 18611–18621.
[78] N. Zhang, S.-S. Han, Y. Xie, D.-L. Chen, W.-D. Yao, X. Huang, W. Liu and S.-P. Guo, *Inorg. Chem.*, 2023, **62**, 7681–7688.
[79] J. Bao, W. Quan, Y. Ning, H. Wang, Q. Wei, L. Huang, W. Zhang, Y. Ma, X. Hu and H. Tian, *Inorg. Chem.*, 2023, **62**, 1086–1094.
[80] Z. Zhijie, L. Deben, H. Hao, C. Yaoqing and X. Jiayue, *Inorg. Chem.*, 2023, **62**, 9240–9248.
[81] Y. Chi, T.-F. Jiang, H.-G. Xue and S.-P. Guo, *Inorg. Chem.*, 2019, **58**, 3574–3577.
[82] Y. Chi, L.-Z. Rong, N.-T. Suen, H.-G. Xue and S.-P. Guo, *Inorg. Chem.*, 2018, **57**, 5343–5351.
[83] W. Zhou, W.-D. Yao, R.-L. Tang, H. Xue and S.-P. Guo, *J. Alloys Compd.*, 2021, **867**, 158879.
[84] A. Sarkar, A. Das, S. Ash, K. V. Ramanujachary, S. E. Lofland, N. Das, K. Bhattacharyya and A. K. Ganguli, *Inorg. Chem.*, 2023, **62**, 9324–9334.
[85] Y. Xiao, S.-H. Zhou, R. Yu, Y. Shen, Z. Ma, H. Lin and Y. Liu, *Inorg. Chem.*, 2021, **60**, 9263–9267.
[86] X. Huang, S.-H. Yang, W. Liu and S.-P. Guo, *Inorg. Chem.*, 2022, **61**, 12954–12958.
[87] V. Werner, U. Aschauer, G. J. Redhammer, J. Schoiber, G. A. Zickler and S. Pokrant, *Inorg. Chem.*, 2023, **62**, 6649–6660.
[88] M. Zhou, K. Xiao, X. Jiang, H. Huang, Z. Lin, J. Yao and Y. Wu, *Inorg. Chem.*, 2016, **55**, 12783–12790.
[89] M. Zhou, X. Jiang, X. Jiang, K. Xiao, Y. Guo, H. Huang, Z. Lin, J. Yao, C.-H. Tung, L.-Z. Wu and Y. Wu, *Inorg. Chem.*, 2017, **56**, 5173–5181.
[90] O. Almora, C. I. Cabrera, J. Garcia-Cerrillo, T. Kirchartz, U. Rau and C. J. Brabec, Adv. Energy Mater., 2021, **11**, 2100022.
[91] M. Mutailipu, J. Han, Z. Li, F. Li, J. Li, F. Zhang, X. Long, Z. Yang and S. Pan, *Nat. Photonics*, 2023, **17**, 694–701.
[92] H. Qiu, F. Li, Z. Li, Z. Yang, S. Pan and M. Mutailipu, J. Am. Chem. Soc., 2023, 145, 24401–24407.